Geophysical Journal International

Geophys. J. Int. (2012) **190,** 442–456 doi: 10.1111/j.1365-246X.2012.05502.x

Teleseismic earthquake swarms at ultraslow spreading ridges: indicator for dyke intrusions?

V. Schlindwein

Alfred Wegener Institute for Polar and Marine Research, Am Alten Hafen 26, D-27568 Bremerhaven, Germany. E-mail: Vera.Schlindwein@awi.de

Accepted 2012 April 11. Received 2012 April 11; in original form 2011 November 3

SUMMARY

Earthquakes at mid-ocean ridges reflect the active magmatic and tectonic processes that form new oceanic crust. Studies of large earthquakes observed on land and smaller earthquakes observed locally or regionally by ocean bottom seismometers or autonomous underwater hydrophones have greatly contributed to our understanding of the structure and active spreading processes at the mid-ocean ridges of the Atlantic and Pacific Ocean opening with velocities in excess of 25 mm yr^{-1}. At spreading rates below 20 mm yr^{-1} full rate, the appearance and the accretion processes of mid-ocean ridges undergo fundamental changes as the melt supply is drastically reduced. The active spreading processes at these so-called ultraslow spreading ridges are still poorly known, as the main representatives, the Arctic Ridge System and the Southwest Indian Ridge, are poorly accessible and neither autonomous underwater hydrophone nor ocean bottom seismometer records of local seismicity are available. In an attempt to compare on a large scale the accretion style of ultraslow spreading ridge sections, I analyse the teleseismically recorded seismicity in 11 sections of the Arctic Ridge System and the Southwest Indian Ridge spanning altogether 7200 km. Epicentres located within 30–35 km of the rift axis were extracted from the catalogue of the International Seismological Centre for a time period of 35 yr. On the basis of a single-link cluster analysis, I identified 27 swarms with eight or more events. These swarms occur almost exclusively at centres of focussed magmatism suggesting that the swarms are probably initiated by magmatism. Normal faults along several tens of kilometres surrounding the volcanic centres react in large earthquakes ($M > 5$) to dyke emplacement. The routine generation of large earthquakes in the cold, brittle lithosphere of ultraslow spreading ridges makes the teleseismic record a valuable means to study ultraslow accretion processes and to provide a global framework for the interpretation of the limited local and regional seismicity studies.

Key words: Seismicity and tectonics; Mid-ocean ridge processes; Submarine tectonics and volcanism; Arctic region; Indian Ocean.

1 INTRODUCTION

Teleseismic studies of mid-ocean ridge earthquakes provided already in the 1960s fundamental insight into the active spreading processes (e.g. Sykes 1967; Francis 1968). Despite the large distance of thousands of kilometres between the earthquake hypocentres at mid-ocean ridges and the nearest recording stations on land, the principal properties of mid-ocean ridge seismicity, like the concentration of shallow normal faulting earthquakes along the rift zones (Sykes 1969) or the dependence of the maximum depth of faulting on the spreading rate (Solomon *et al.* 1988), could be established from teleseismic earthquake records. Earthquake swarms at mid-ocean ridges were already known since the 1970s (Sykes 1970). However, detailed studies of the spatial and temporal properties of such swarms using teleseismic records faced problems with the high detection threshold for the distant mid-ocean ridge earthquakes and the limited location accuracy despite relocation efforts (e.g. Bergman & Solomon 1990; Korger & Schlindwein 2012). Since the late 1980s, local earthquake studies using ocean bottom seismometers (OBS; e.g. Toomey *et al.* 1985; Wolfe *et al.* 1995; Tolstoy *et al.* 2008) and regional studies using autonomous underwater hydrophones (AuH; e.g. Fox *et al.* 1995; Smith *et al.* 2003; Simao *et al.* 2010) have greatly contributed to a detailed understanding of mid-ocean ridge seismicity (see Rundquist & Sobolev 2002 and Bohnenstiehl & Dziak 2008 for comprehensive reviews). With the low detection threshold of AuHs of $M \sim 2$ it even became possible to monitor low magnitude seismic swarms accompanying the emplacement of dykes (e.g. Dziak *et al.* 1995; Fox & Dziak 1998).

However, these studies have mainly concentrated on the ridge systems of the Atlantic and Pacific Oceans as these are easily accessible. Our detailed knowledge about active spreading processes at

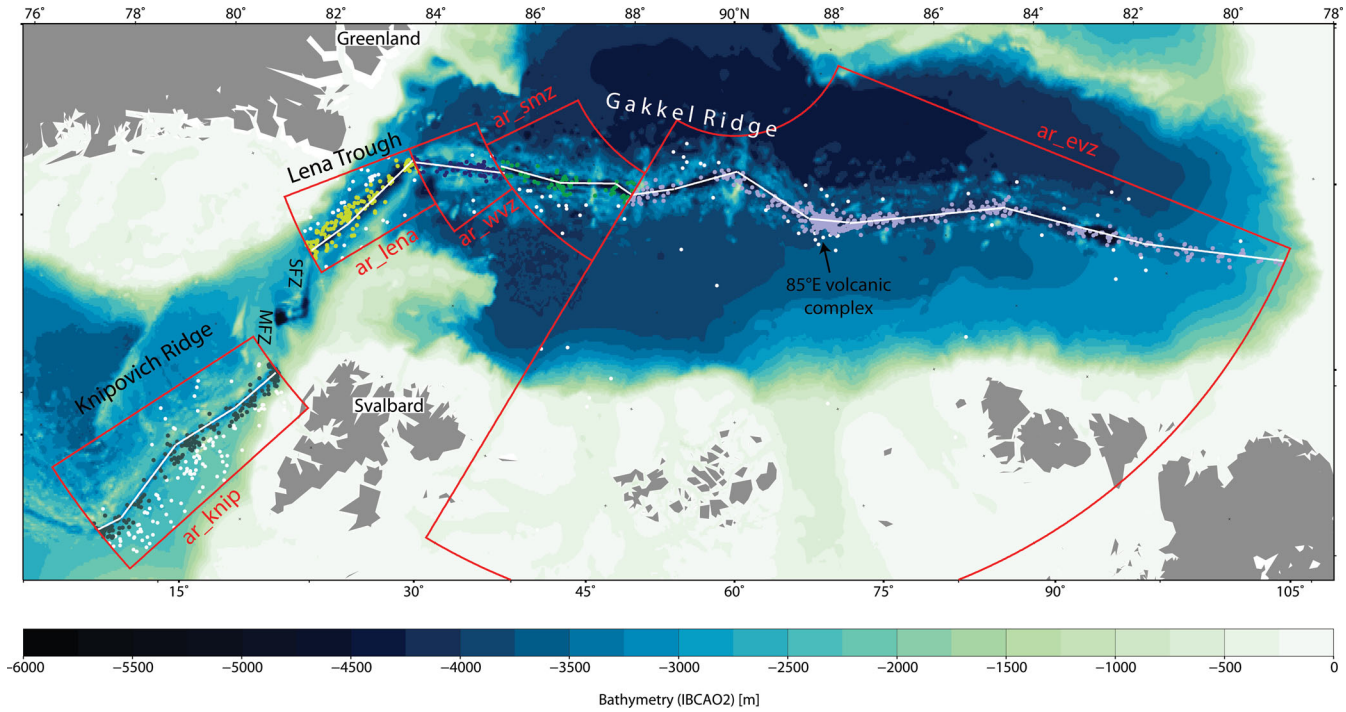

Figure 1. Map of the Arctic Ridge System (ARS). The five studied sections are labelled and marked with red boxes used for earthquake extraction from the ISC catalogue. Only earthquakes within 30 km of the rift axis (white line) are used. White circles: unused earthquakes; coloured circles: earthquakes included in this study. The section colours are used consistently in Figs 3 and 7. Bathymetry is IBCAO2 (Jakobsson *et al.* 2008). Main topographic features are labelled. MFZ, Molloy Fracture Zone; SFZ, Spitsbergen Fracture Zone.

mid-ocean ridges therefore refers to ridges with full spreading rates in excess of ∼25 mm yr^{-1}. Below 20 mm yr^{-1}, the nature of accretion processes at mid-ocean ridges undergo fundamental changes as conductive cooling of the ultraslow spreading lithosphere drastically reduces the amounts of melt available to form the new ocean crust (e.g. Bown & White 1994). Dick *et al.* (2003) defined ultraslow spreading ridges with spreading rates <20 mm yr^{-1} as a new class of mid-ocean ridges with distinct morphology, petrology and physical properties that distinguish these ridges from faster spreading ridges. The routine exploration of ultraslow spreading ridges, which constitute about 10 per cent of the worldwide system of mid-ocean ridges, has long been prevented, basically for logistic reasons. The main representatives of this class of mid-ocean ridge are the Arctic ridge system (ARS; Fig. 1) with perennial sea-ice cover and the Southwest Indian Ridge (SWIR; Fig. 2) experiencing extreme weather conditions. Geological mapping of these ridges since the late 1990s showed that magmatism at ultraslow spreading ridges is present despite low melt supply, but it is focussed in discrete volcanic centres with stretches of non-volcanic seafloor in between (see Dick *et al.* 2003; Michael *et al.* 2003; Sauter & Cannat 2010 and references within for comprehensive reviews). Segments with robust magmatism resembling the slow spreading Mid-Atlantic ridge (MAR) alter with amagmatic segments and segments with focussed magmatism, their spatial distribution being not a function of spreading rate (Michael *et al.* 2003). Up to date very little is known about the active spreading processes operating at ultraslow spreading ridges as neither routine AuH monitoring nor dedicated local OBS studies were feasible at these remote ridges. The teleseismic observation of a strong earthquake swarm at eastern Gakkel ridge in 1999 (Fig. 1; Müller & Jokat 2000; Tolstoy *et al.* 2001) together with indications of hydrothermal event plumes (Edmonds *et al.* 2003) and explosive volcanism (Sohn *et al.* 2008) demonstrated that active magmatic accretion at an ultraslow spreading mid-ocean ridge may drastically differ from dyking episodes known from faster spreading ridges underlining the need of comprehensive seismicity studies of ultraslow-spreading ridges. The detection of explosive seismoacoustic sounds with seismometers on ice near the 85°E volcano at eastern Gakkel ridge in 2001 (Schlindwein *et al.* 2005) motivated an intensive reanalysis of the teleseismically observed earthquake swarm in 1999 (Riedel & Schlindwein 2010; Schlindwein & Riedel 2010; Korger & Schlindwein 2012) and underlined its differences in magnitude and duration to seismic swarms observed at faster spreading ridges (e.g. Dziak *et al.* 1995). Repeated swarm activity at the western SWIR was detected by the Neumayer seismic array in Antarctica between 2001 and 2009 (Läderach *et al.* this issue). This observation further showed that earthquake swarms at ultraslow spreading ridges might be more common than expected from the reduced melt supply. To better understand the nature, relevance and spatial distribution of earthquake swarms at ultraslow spreading ridges and their relation to potential spreading episodes, this study performs a systematic analysis of spatial and temporal earthquake clusters of the ARS and the SWIR. In the absence of AuH monitoring in the Arctic and Southern Indian Ocean, it has to fall back on teleseismic records, using 35 yr of teleseismic data from 7200 km of ridge axis at ultraslow spreading ridges.

2 METHODS

2.1 Extraction of earthquakes

2.1.1 Definition of ridge sections

The ARS and the SWIR can be divided in 11 large-scale ridge sections with specific morphological and geological properties (ARS:

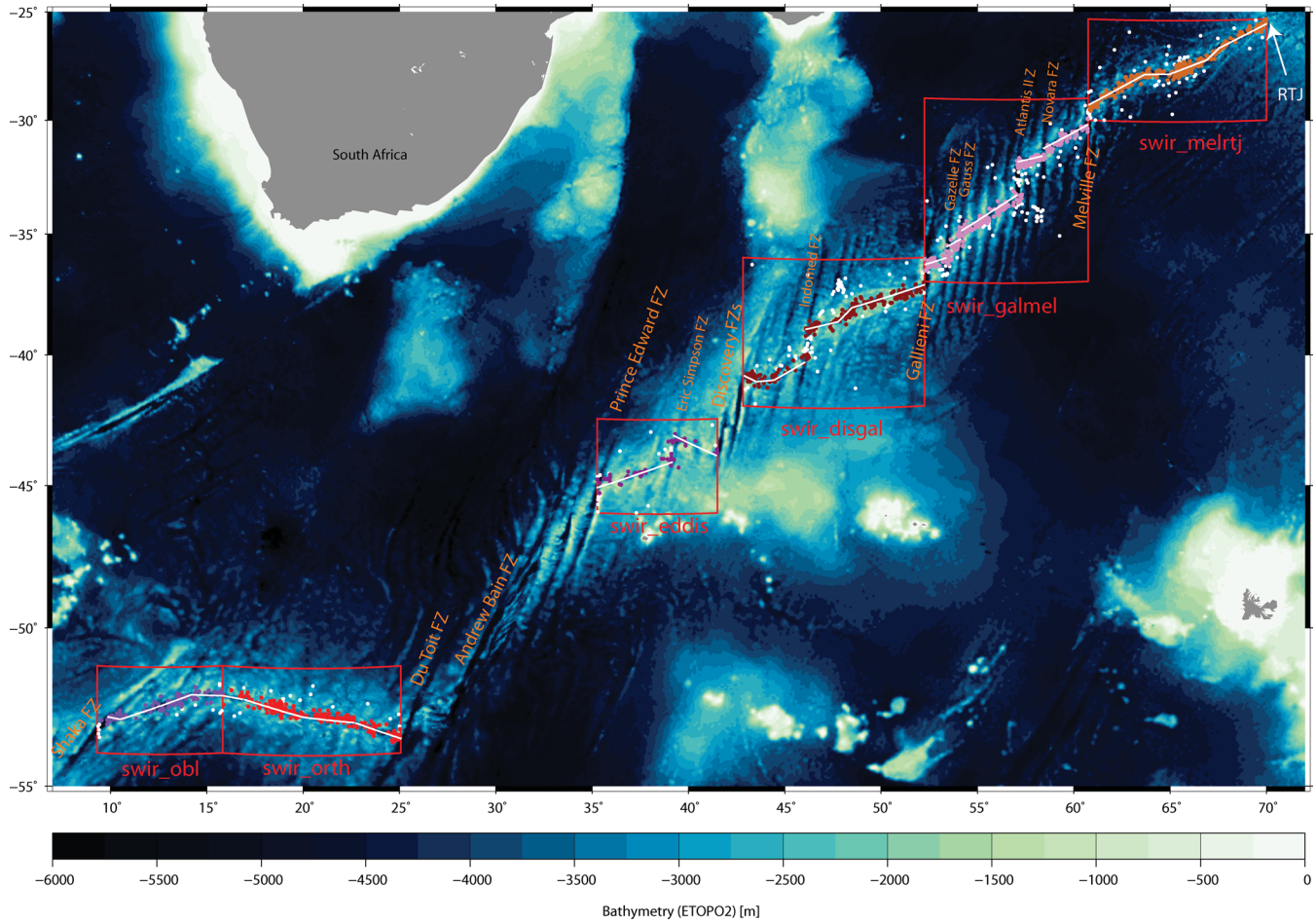

Figure 2. Map of the Southwest Indian Ridge (SWIR). The six studied sections are labelled and marked with red boxes used for earthquake extraction from the ISC catalogue. Only earthquakes within 35 km of the rift axis (white line) are used. White circles: unused earthquakes; coloured circles: earthquakes included in this study. The section colours are used consistently in Figs 3 and 7. Bathymetry is ETOPO2 (Smith & Sandwell 1997). Main topographic features are labelled. RTJ, Rodriguez Triple Junction.

Michael *et al.* 2003; SWIR: Mendel *et al.* 2002; Dick *et al.* 2003; Figs 1 and 2); namely the Knipovich Ridge (abbreviated in the following as ar_knip), the Lena Trough (ar_lena), the Western Volcanic Zone (ar_wvz), the Sparsely Magmatic Zone (ar_smz), and the Eastern Volcanic Zone (ar_evz) at the ARS, and on the SWIR the Oblique Supersegment (swir_obl), the Orthogonal Supersegment (swir_orth), the ridge section between the Prince Edward Fracture Zone (FZ) and the Discovery FZ (swir_eddis), between the Discovery FZ and the Gallieni FZ (swir_disgal), between the Gallieni FZ and the Melville FZ (swir_galmel) and between the Melville FZ and the Rodriguez Triple Junction (swir_melrtj). The transform-dominated ridge portions between ar_knip and ar_lena (Molloy FZ, Fig. 1) and between the Andrew Bain FZ and the Prince Edward FZ (Fig. 2) are not considered in this study of accretion processes. A summary of section lengths, spreading rates and average water depths is found in Table 1.

The red boxes in Figs 1 and 2 mark the latitude and longitude range around each section for which earthquakes were extracted from the bulletin of the International Seismological Centre (ISC; International Seismological Centre 2001). The boxes define the sections' boundaries along-axis and extend for at least 50 km off-axis to include all earthquakes. For each section, I defined a reference line, which roughly follows the centre of the rift valley. These reference lines are used to calculate the distance of the earthquake epicentres to the ridge axis and to construct along-axis transects of seismicity while reflecting roughly the along-axis topography of the ridge. The reference line does not attempt to define the actual plate boundary. In cases of subparallel troughs or fault blocks protruding into the rift valley, the reference line may traverse ridge shoulders. To project all earthquakes onto the reference line it was important that it spans the entire length of a section without overlaps and that it is only offset at first order discontinuities (Fig. 2). I used the tools of

Table 1. Ridge section lengths, water depths and spreading rates at centre of section (DeMets *et al.* 1994).

Segment	Length (km)	Mean depth (km)	Full spreading rate (mm yr^{-1})
ar_knip	529	3.227	14.5
ar_lena	304	4.120	13.5
ar_wvz	201	3.700	12.7
ar_smz	305	4.571	12.0
ar_evz	1501	4.069	10.2
swir_obl	420	3.828	13.5
swir_orth	634	3.850	13.8
swir_eddis	530	2.453	14.1
swir_disgal	883	3.104	14.1
swir_galmel	882	3.987	14.0
swir_melrtj	1019	4.476	13.6

GeoMapApp (http://www.geomapapp.org) which incorporates the Global Multi-Resolution Topography Synthesis of Ryan *et al.* (2009) to zoom in on the bathymetry, visually define the reference line and extract the geographical coordinates and water depths along this line.

2.1.2 Compilation of an earthquake catalogue

To compile a uniform teleseismic earthquake catalogue for the 11 ridge sections, I extracted for each of the boxes in Figs 1 and 2 earthquake data from the ISC catalogue as follows: For the period 1.1.1976–31.12.2008 epicentres with a solution calculated by the ISC were used. For the period from 2009 January 1 to 2010 December 31 I used IDC solutions as ISC solutions are not yet available. The extraction boxes contain additional seismicity which is not related to spreading processes, either resulting from transform motion or, like at the eastern side of ar_knip, from other tectonic processes, in this case vertical motion due to sediment loading (Faleide, personal communication, 2011). I therefore limited the data set to earthquakes with distances of less than 30 km to the rift axis transect for the ARS and 35 km for the SWIR. The larger distance for SWIR was used because the average location error of earthquakes at the SWIR is larger than at the ARS (Table 2). The distribution of number of events versus distance to the ridge axis tails off at 35 km distance for the SWIR. The extracted data set contains 1021 events for the ARS and 1346 events for the SWIR (Figs 1 and 2, Table 2). I added all available moment tensor solutions from the GCMT catalogue (Ekström *et al.* 2005) to the data set.

Transform fault seismicity is mostly excluded for transforms with offsets larger than 70 km (e.g. Indomed FZ, Atlantis II FZ), but transform-related seismicity at ridge-transform intersections is present in the data set. As moment tensor solutions exist only for large earthquakes, discrimination between normal fault and strike-slip earthquakes is not possible for smaller events. Therefore, it is important to bear in mind that the compiled data set contains a small part of transform-related seismicity.

Fig. 3 shows the seismicity over time for all 11 ridge sections. Earthquakes were projected orthogonally onto the rift axis reference line and plotted over along-axis distance. The number of detected events increased markedly after 1995. Table 2 summarizes the quality of the data set. The detection capability of earthquakes at the SWIR is worse than at the ARS but it improved since 1995. At the SWIR, the average number of phases used for earthquake location decreased since the improvement of the global seismic network in the mid-1990s (Table 2) resulting in an increased error of the epicentre solutions. At the same time, the average magnitude of the earthquakes at the SWIR decreased implying that the apparent deterioration of the catalogue for the SWIR mainly results from the inclusion of many smaller events. The ARS catalogue also comprises more small events since 1995, but station coverage and localization quality has been constant over time.

For each event I calculated the unified magnitude M_u following the procedure of the ISC (Scordilis 2006): If M_w was reported, M_u was set equal to M_w. If M_w was not available, but M_s was reported, I used

$$\begin{aligned} M_u &= 0.67M_s + 2.07 (M_s < 6.2) \\ M_u &= 0.99M_s + 0.08 (M_s \geq 6.2). \end{aligned} \quad (1)$$

For all other events, M_u was calculated from m_b as

$$M_u = 0.85m_b + 1.03. \quad (2)$$

I derived the seismic moment M_0 in Nm for each event from its unified magnitude M_u, using

$$M_u = \frac{2}{3}(\log M_0 - 9.1) \quad (3)$$

(Kanamori 1977). Normalized over the rift axis length and the observation period this yielded the moment release rate.

2.2 Single-link cluster analysis

To identify clusters of seismicity in time and space, I used the single-link cluster analysis technique of Frohlich & Davis (1990). The algorithm establishes links between all earthquakes and calculates a link length in space and time defined as

$$d_{st} = \sqrt{d^2 + C^2t^2}, \quad (4)$$

where d is the distance in kilometres between two epicentres and t is the time difference between their origin times in days. For teleseismic events, Davis & Frohlich (1991) suggest $C = 1\,\text{km d}^{-1}$. For each event, the nearest neighbour is found with the minimum d_{st}. Two events are considered as clustered if their link d_{st} is smaller than

$$D = 9.4\text{km}^{\frac{1}{2}}\sqrt{S1} - 25.2\,\text{km}, \quad (5)$$

where S1 is the median of all minimum d_{st} values. For the ARS, I obtained $D = 23.93$ km, for the SWIR with larger scattering of epicentres $D = 33.155$ km. Using this cut-off criterion, the program is then used recursively until all subgroups of clustered events are joined into clusters where each event has at least one neighbour with a link shorter than D. This procedure was applied to each of the 11 sections separately. The results are shown in Fig. 4.

On the basis of the single-link cluster analysis, I further compiled a declustered seismicity catalogue. This catalogue contains all single events and the first event of each cluster regardless of the magnitude of this event. The event rate (number of events per km rift axis and year) in bins of 20 km along the rift axis for the complete and the declustered catalogues was used to illustrate sites of increased seismicity relative to the background rate (Fig. 5).

Table 2. Quality of the earthquake data sets for the ARS and SWIR.

Ridge	Number of events	Mean M_u	Mean distance to rift axis (km)	Mean location error Smaj (km)	Mean number of phases
ARS total	1021	4.58	10.0	12.4	70.7
SWIR total	1346	4.77	11.8	31.1	29.0
ARS before 1995	240	4.93	10.4	8.6	72.3
SWIR before 1995	287	5.19	12.2	12.8	43.3
ARS since 1995	781	4.47	9.9	13.5	70.2
SWIR since 1995	1059	4.66	11.7	36.1	25.1

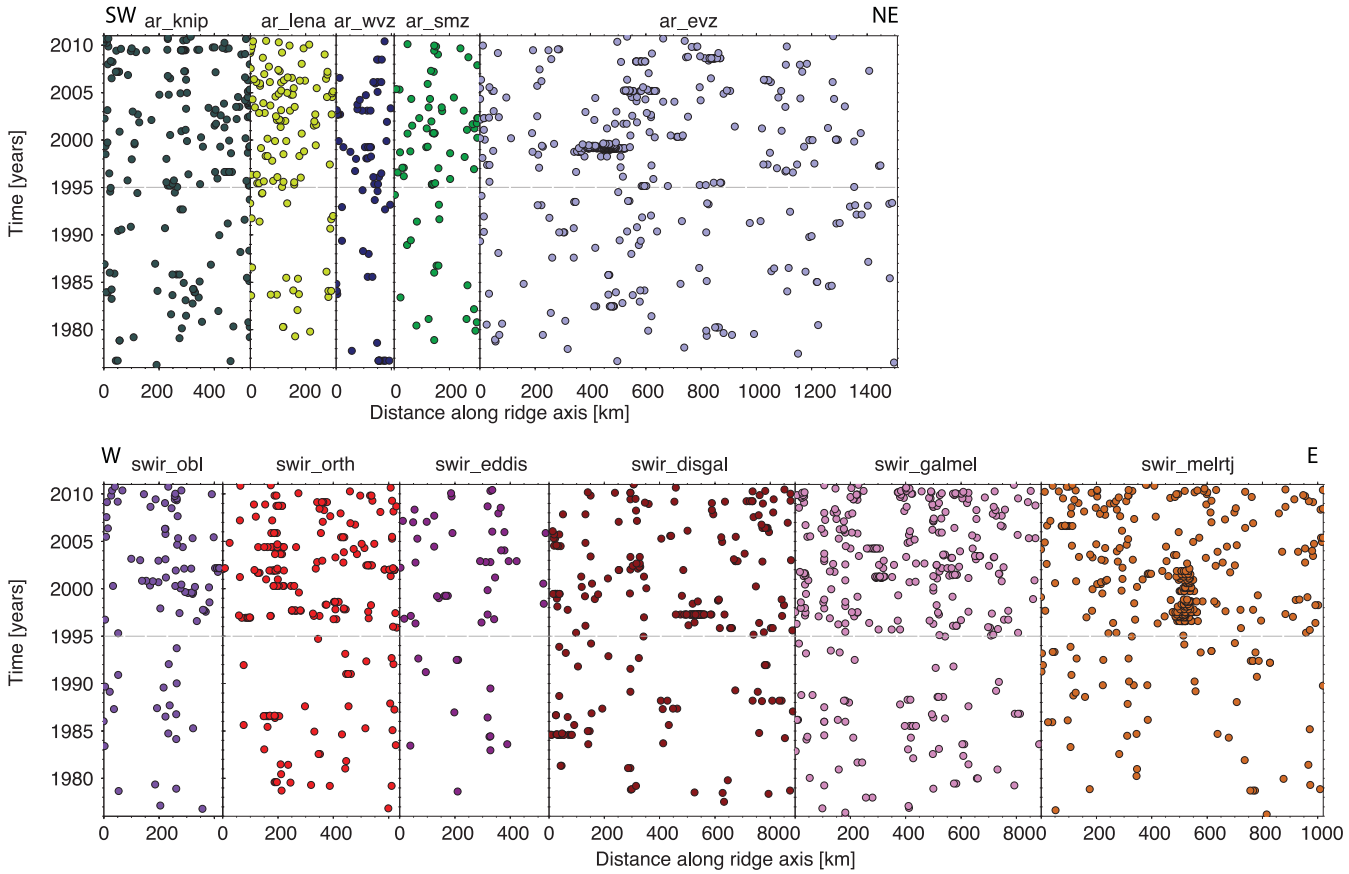

Figure 3. Seismicity over time and distance along the ridge axis for all ridge sections. The same colours as in Figs 1 and 2 are used to distinguish between the ridge sections. Note the increased number of earthquakes since 1995 due to a lower detection threshold.

3 DESCRIPTION OF RESULTS

3.1 Definition of seismic swarms

The definition of a seismic swarm is somewhat arbitrary. In aftershock sequences, magnitude and frequency of earthquakes following a mainshock gradually decrease over time (Mogi 1963). Swarms, in contrast, are a group of events without a mainshock. McNutt (1996) stresses that tectonic events at volcanoes tend to occur in swarms rather than in aftershock sequences. He observes that the largest and the second largest event of a swarm differ in magnitude by only about 0.5, whereas a mainshock exceeds all events of an aftershock sequence by more than one magnitude unit. Bohnenstiehl & Dziak (2008) call swarms periods of sustained earthquake activity with the total number of events in a swarm exceeding the variance of the background seismicity by more than 10 per cent.

Given the high detection threshold of the teleseismic catalogue, it is likely that mainshock–aftershock sequences with rapidly decreasing magnitudes produce clusters with only few earthquakes above the detection threshold whereas swarms may produce several moderately sized earthquakes, which are recordable at teleseismic distances. I therefore assume that clusters with larger numbers of events are more likely to be of swarm-type without a mainshock than shorter clusters. Fig. 4 shows the distribution of event numbers in the clusters. Starting with 130 clusters consisting of two events, the number of clusters quickly and continuously decreased with increasing cluster size to only four clusters consisting of seven events. Clusters with 9 and 10 events were again more numerous. A number of eight events therefore appeared to mark a break in the cluster size distribution. In the following, I call a cluster with eight or more earthquakes a 'swarm' regardless of its magnitude-time evolution. Swarms appear in yellow in all seismicity plots (Figs 4 and 5). Clusters with 2–7 events are referred to as 'sequences' and are plotted in orange, whereas single events are plotted in dark red. Fig. 4 shows the percentage of earthquakes of each type for the individual ridge sections. The data set contained 27 swarms with eight or more events which are described in Table 3 and analysed in more detail in the following.

3.2 Locations of teleseismic earthquake swarms

The earthquake swarms occurred at 12 discrete sites, which I describe in the following in context with rift morphology, petrology and the character of the central magnetic anomaly (CMA) at the spreading axis (Table 3; Fig. 5). Fig. 6 shows an example of a seismicity map with bathymetry and CMAs for section ar_evz. Equivalent maps for the other sections are included in the Supporting Information (Figs S1–S6). While all of the swarm locations show evidence for magmatic accretion, the level of available information varies markedly.

(1) Section ar_knip hosts a small swarm of low-magnitude events where the detailed bathymetry of Okino *et al.* (2002) shows a pair of elevated rift shoulders at both sides of the rift valley interpreted by Curewitz *et al.* (2010) as symmetric chain of off-axis highs.

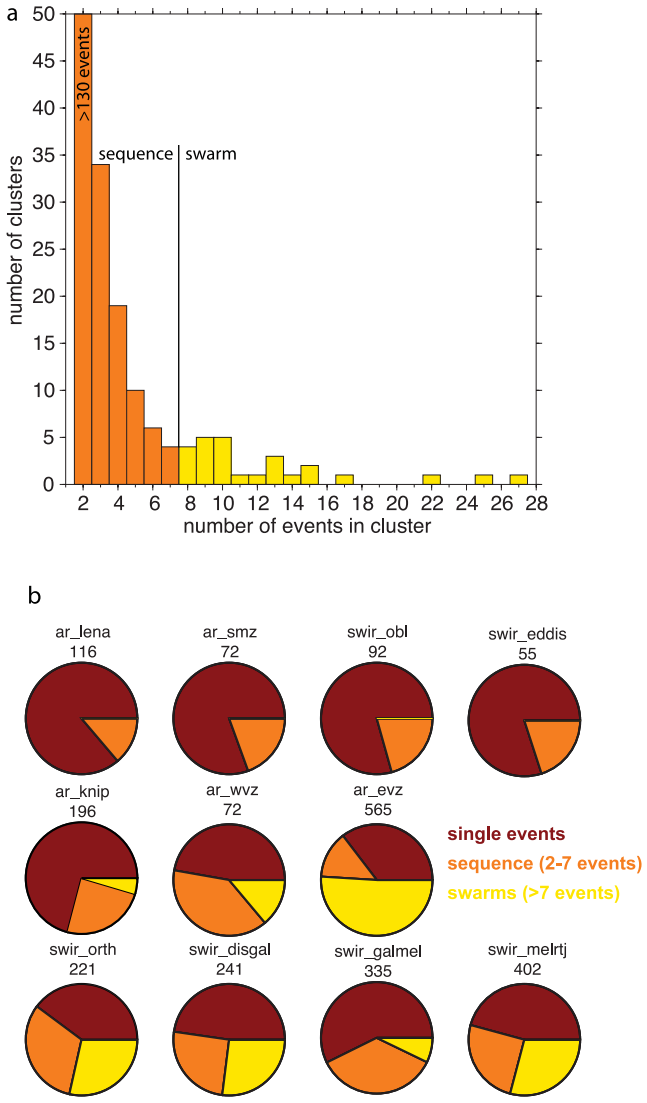

Figure 4. Results of the single-link cluster analysis. (a) Histogram of cluster size distribution. Clusters with eight or more events are called swarms and analysed in this study. (b) Proportion of single events, events in sequences and swarms in each section. Total number of analysed events is indicated above each diagram together with section name. Sections in the top row lack swarms and are not further studied here.

Comparable topographic highs are associated to the north with the Logachev Seamount (Fig. S1). Neither a pronounced axial volcanic ridge (AVR) nor a CMA were observed at this site. Its volcanic nature therefore remains somewhat unclear.

(2) The entire section ar_wvz is seismically active with many events organized in clusters or swarms (Fig. 5). The seismicity coincides with a continuous pronounced CMA (Fig. S2) along the rift axis which is evident also in the high-resolution magnetic data of Jokat & Schmidt-Aursch (2007). A swarm of 10 strong events is located at the eastern end of this segment. Basalts were dredged at this site but a pronounced AVR is absent.

(3) Section ar_evz hosts four swarm sites (Fig. 6). Circular CMAs, AVRs visible in the along-axis topography or symmetric chains of off-axis highs extending for several tens of kilometres perpendicular to the spreading axis (Figs 5 and 6) characterize the swarm sites. Towards the east, site 6 is more difficult to identify to due an increasing sediment cover. Of particular interest are the 85°E volcanic complex (site 3) and the neighbouring Eastern Volcano at about 93° (site 4) where high reflectivity of ocean floor was interpreted to indicate recent volcanic activity (Edwards *et al.* 2001). The entire rift section between kilometres 400 and 650 (Fig. 5) released five seismic swarms between 1982 and 2008, the 1999 earthquake swarm at site 3 being the largest ever recorded mid-ocean ridge earthquake swarm marking the onset of a volcanic cycle which persisted at least throughout 2001 (Schlindwein & Riedel 2010). The swarm site showed signs of recent explosive volcanism (Sohn *et al.* 2008).

(4) Section swir_orth displayed repeated seismic swarms concentrated at about 18°–19°E (site 7). The Neumayer seismic array in Antarctica is situated in a favourable location to record earthquakes from this portion of the ridge resulting in a detection threshold of about magnitude 3.2 (Läderach *et al.* this issue). In that study, we show that all seismic swarms detected by the array between 2001 and 2009 are also seen teleseismically. The swarm site shows a continuous CMA (Fig. S3), basalts at the seafloor and a mantle Bouguer anomaly low. As at site 2, a prominent AVR is not present.

(5) East of about 49°, previous studies have divided the ridge in distinct short segments centred at individual AVRs (Cannat *et al.* 1999). Relevant segments are numbered in Fig. 5. At section swir_disgal, the second largest swarm (42 events) found in this study is situated at segment 30 near a large non-transform discontinuity, which offsets the CMA (site 9). West of the Indomed FZ, the CMA is considerably weaker apart from a patch near the Discovery FZs which hosts two smaller earthquake swarms (site 8) with strong normal fault events despite the proximity to the transform fault (Fig. S4).

(6) The rift axis in section swir_galmel (Fig. S5) is offset by numerous FZs. Between the FZs, the rift axis shows a continuous CMA, several large AVRs associated with mantle Bouguer anomalies. Segments 20 and 21 are seismically most active featuring two swarms at segment 21 during the survey period (site 10).

(7) The easternmost ridge section swir_melrtj (Fig. S6) has no transform discontinuities and a less stable segmentation pattern than swir_galmel. Nevertheless, a number of well-defined AVRs represent sites of crustal accretion (Fig. 5). A single swarm is associated with segment 14 (site 11) but repeated swarm activity occurred at segment 8 over 7 yr (site 12). The earthquakes here coincide with a pronounced magnetic anomaly, which is located slightly east of the crest of the AVR (Sauter *et al.* 2004a).

In summary, there is solid evidence that earthquake swarms of eight or more events occur at sites of magmatic accretion. No swarm activity is observed in rift sections with predominantly amagmatic extension such as ar_lena, ar_smz and swir_obl (Fig. 4). In these rift sections, peridotite is exposed at many places at the seafloor (Dick *et al.* 2003; Michael *et al.* 2003; Snow *et al.* 2011).

3.3 Swarm analysis

In the following, I analyse in more detail the 27 swarms of eight or more earthquakes as retrieved from the cluster analysis. Fig. 7 summarizes the swarm characteristics. The majority of the swarms last less than 10 days, count less than 20 teleseismically recorded earthquakes and release a total seismic moment of about 10^{18} Nm. These three parameters are not correlated in a systematic way with each other. The moment release of a swarm neither depends on its number of events nor on its duration. There is also no preferential swarm size or duration of particular ridge sections. The earthquake swarm of 1999 at the 85°E volcanic complex is in every respect

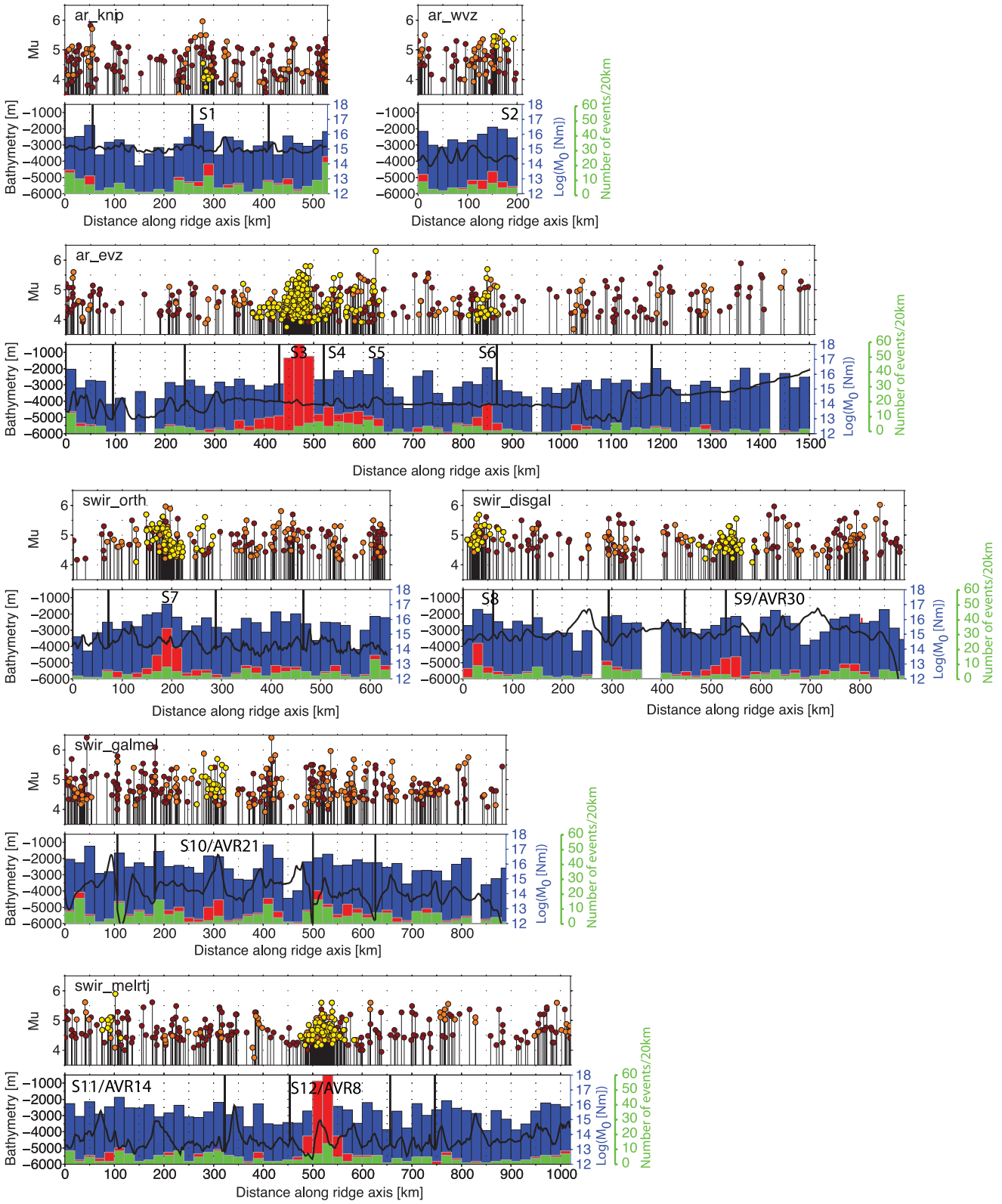

Figure 5. Along-axis seismicity and swarm locations for all sections with seismic swarms. Top panel: unified magnitudes. Colours indicate single events (dark red), sequences (orange) and swarms (yellow). Bottom panel: seismic moment release (blue), number of all events (red) and number of declustered events (green) in bins of 20 km. Black line: topographic relief along the rift reference line as defined in Figs 1 and 2. Vertical black lines indicate offsets or direction changes of the reference line. The swarm sites (Table 3) are labelled S1–S12. AVR indicates the segment number as defined in Cannat *et al.* (1999).

Table 3. Summary of swarm characteristics.

Section	Swarm site (profile km; coordinates)	Geology	Swarm date	# events	Mu_{max1}	$Mu_{max1} - Mu_{max2}$
ar_knip	1 (km 296; 76.2°N/08°E)	sc[1,2]	06/2009	9	4.55	0.27
ar_wvz	2 (km 170; 84.3°N/01°E)	coMa, b[3,4]	09/1976	10	5.62	0.17
ar_evz	3 (km 475; 85.7°N/86°E)	avr, b, ciMa[4,5]	06/1982	8	5.55	0.20
			01/1999	220	5.80	0.00
	4 (km 550; 85.3°N/93°E)	ciMa, avr[5–7]	08/03/2005	13	5.50	0.10
			04/2008	12	5.10	0.10
	5 (km 625; 84.9°N/100°E)	ciMa, avr[5,7]	06/03/2005	8	6.30	**1.00**
	6 (km 850; 83.5°N/114°E)	sc[7]	08/2008	27	5.70	0.30
swir_orth	7 (km 190; 52.5°S/19°E)	coMa, b, mba[5,8,9]	07/1986	15	5.69	0.07
			09/1997	8	5.60	0.30
			04/2000	8	5.08	0.31
			12/2001	9	5.60	**0.72**
			05/2004	13	5.40	0.20
			09/2008	10	5.02	0.40
swir_disgal	8 (km 30; 40.9°S/43°E)	ciMa[5]	07/1984	13	5.69	0.14
			06/1999	10	5.30	0.15
	9 (km 550; 38.0°S/49°E)	coMa, avr30, b [5,10,11]	04/1997	42	5.55	0.25
swir_galmel	10 (km 310; 34.3°S/55°E)	sc, avr21, ciMa, mba, b[10–13]	04/2001	15	5.50	0.10
			03/2004	9	5.70	0.30
swir_melrtj	11 (km 90; 28.8°S/61.5°E)	sc, b, avr14, mba, ciMa[5,11,14,15]	08/2006	10	5.90	**0.80**
	12 (km 510; 27.6°S/65.5°E)	b, avr8, mba, ciMa[16]	07/1996	22	5.60	**0.50**
			12/1996	9	5.22	0.34
			04/1997	9	4.75	0.07
			07/1997	25	5.08	0.20
			08/1998	14	5.03	0.21
			09/1999	11	5.00	0.10
			02/2000	17	5.60	0.30

Notes. sc, symmetric chain of off-axis highs; coMa, continuous central magnetic anomaly; b, basalt; avr, axial volcanic ridge (number indicates segment number at SWIR after Cannat *et al.* (1999)); ciMa, circular central magnetic anomaly; mba, mantle Bouguer anomaly low.
[1]Curewitz *et al.* (2010). [2]Okino *et al.* (2002). [3]Jokat & Schmidt-Aursch (2007). [4]Michael *et al.* (2003). [5]Maus *et al.* (2009). [6]Edwards *et al.* (2001). [7]Jakobsson *et al.* (2008). [8]Grindlay *et al.* (1998). [9]Dick *et al.* (2003). [10]Cannat *et al.* (1999). [11]Meyzen *et al.* (2005). [12]Sauter *et al.* (2001). [13]Sauter *et al.* (2004b). [14]Cannat *et al.* (2008). [15]Rommevaux-Jestin *et al.* (1997). [16]Sauter *et al.* (2004a).

abnormal, counting 210 events in 213 days and releasing 6.57×10^{18} Nm seismic moment.

The comparison with the regionally observed swarms at the Neumayer array (Läderach *et al.* this issue) showed, that the swarm duration defined from teleseismic earthquakes largely agreed with the swarm duration as defined by the more numerous regionally recorded events. Only one swarm (2001 December) had a preponderance of large events at its beginning and therefore a significantly shorter duration (1.1 days vs. 7.1 days) in the teleseismic record.

To evaluate the character of the swarms it would be helpful to see if the swarms obeyed a power-law decay of the event rate (Modified Omori law; Utsu *et al.* 1995). However, a meaningful analysis of the time dependence of the event rate can only be performed for a significant number of seismic events larger than the magnitude of completeness for the catalogue. This severely restricted the number of events in the present case leaving only two swarms for analysis (see description of applied method in Läderach *et al.* this issue). However, the criterion of McNutt (1996) proved a helpful tool to identify potential mainshock–aftershock sequences. Table 3 lists the magnitude difference between the largest event and the second largest event for each swarm. Four swarms marked in bold have a largest earthquake exceeding all others by at least 0.5 magnitude units. These swarms at site 5, 11 and 12 (07/1996) release most of their seismic moment in the largest earthquake early in the swarm (for moment release histories of all swarms see Fig. S7 in the Supporting Information) and are most likely tectonic mainshock–aftershock sequences. At site 7, the swarm of 12/2001 showed a mainshock, but it occurred very late in the sequence. This swarm was analysed by Läderach *et al.* (this issue) including many smaller regionally recorded events, but the event rate decay could not be approximated by a power-law. Hence, all but three of 27 swarms analysed here are typical swarms with increased seismicity over longer periods without a dominant mainshock and its aftershocks.

To analyse swarm patterns in time and space, I extracted from Fig. 3 examples of spatially extended swarm activity at ar_evz and swir_disgal and examples of repeated swarm activity at swir_orth and swir_melrtj. Fig. 8 includes all event clusters (sequences and swarms) in different colours, but constraints on location quality have been imposed. At ar_evz (Fig. 8, top left-hand side), two instances of almost contemporaneous seismic clusters at adjacent volcanic centres are observed. The 1999 earthquake swarm at the 85°E volcanic complex (km 450–500) was preceded three months before its onset by a sequence of six events at about 75°E (km 350). The area in between appears to be activated during the 1999 earthquake swarm, but relocation of epicentres only could prove an extent of the seismically active area out to about 80°E (Korger & Schlindwein 2012). In 2005, a ridge section of 110 km length was activated in two swarms: It started in the east at km 630 (99°E, site 4) as a tectonic mainshock–aftershock sequence with 10 events on March 6 and 7, including the largest recorded earthquake of M_u 6.3 in this study. One day later, a swarm of 13 events began near km 550 (90°E)

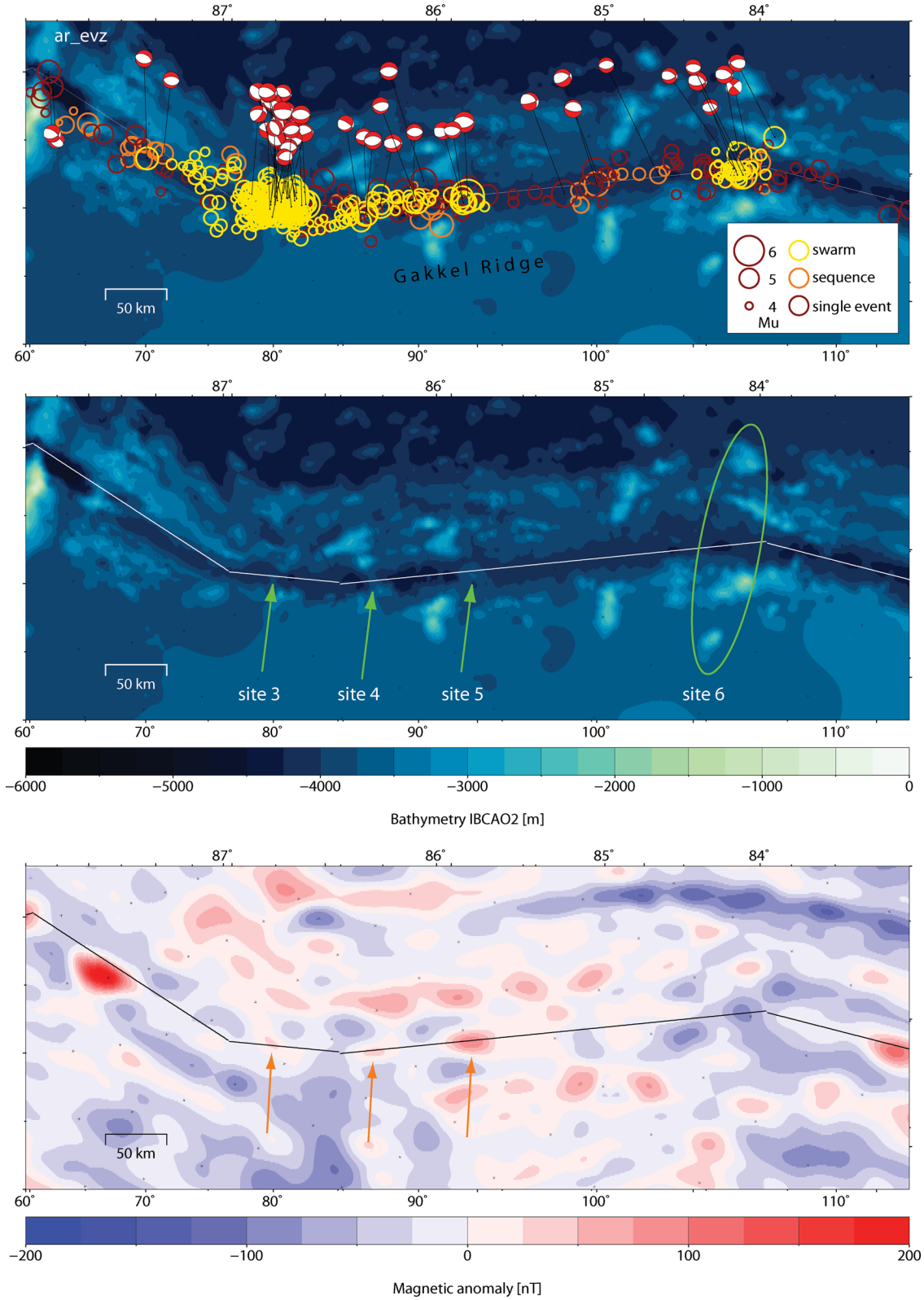

Figure 6. Close-up map of section ar_evz showing swarm sites 3–6. Top panel: bathymetry with seismicity including moment tensor solutions. Middle panel: bathymetry with features of swarm sites indicated. Green arrows mark AVRs. Green ellipse marks symmetric chain of off-axis highs. Bottom panel: EMAG2 magnetic anomaly map (Maus *et al.* 2009) with circular CMA indicated by orange arrows.

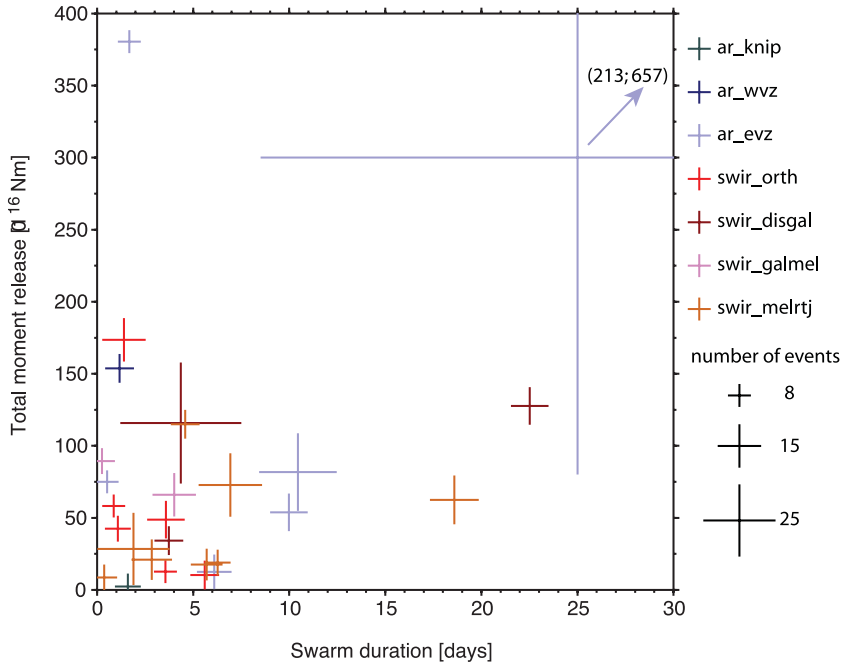

Figure 7. Duration, moment release and event numbers of 27 swarms with eight or more events. Colours refer to sections as indicated. The 1999 earthquake swarm at 85°E (section ar_evz) plots far outside the range of this diagram. The x,y coordinates in brackets indicate the correct position of the cross.

lasting for 10 days with later events being positioned more to the west. This latter swarm clearly did not qualify for a mainshock–aftershock series.

Another example of spatially extended swarm activity was found at segment 30 of swir_disgal affecting a segment length of at least 50 km and up to 120 km depending on epicentre location quality (Fig. 8, bottom left-hand side).

While none of the described spatially extended swarms experienced a comparable repetition during the observation period, segment 8 at swir_melrtj showed a remarkable cluster of repeated seismic sequences which is spatially limited to a region of 80 km at its most (Fig. 8, top right-hand side). Activity started in July 1996 with a tectonic mainshock–aftershock sequence, followed by six swarms of different character and numerous smaller earthquake sequences until July 2003. The time between the clusters is typically a few months up to a year, with particularly short intervals between clusters in the period between February 2000 and November 2001 featuring 55 events altogether. Prior and after this 7 yr period, the region showed no increased levels of seismicity compared to its neighbourhood.

At swir_orth (Fig. 8, bottom right-hand side), a spatially limited segment of 80 km along axis showed seven earthquake clusters between 1986 and 2008, with five clusters between 2000 and 2008. Läderach *et al.* (this issue) relocated the earthquake swarms of 2001–2008 and found that they actually concentrate in a narrow 40 km ridge section along axis.

4 INTERPRETATION OF EARTHQUAKE SWARMS AND DISCUSSION

I hypothesize that the majority of the swarms are closely related in time and space to dyking events. For none of the swarms apart from the unusual 1999 earthquake swarm at Gakkel ridge there is direct evidence for contemporaneous intrusive or extrusive magmatism. However, several lines of evidence support a magmatic origin of the observed earthquake swarms, as follows.

(1) The earthquake swarms occur exclusively at volcanic centres or segments with robust magmatic accretion (swir_orth, ar_wvz).

(2) Most of the swarms lack a mainshock and the subsequent power-law decay of the aftershock rate expected for tectonic earthquake sequences.

(3) The swarms last from days to weeks and exhibit sustained seismicity rates considerably higher than the background seismicity.

(4) Some of the sites show repeated swarm activity at discrete sites (site 8, 12) with repetition patterns similar to dyke intrusion episodes. Site 12 hosted 13 seismic sequences including six swarm-type sequences without a mainshock between 1996 and 2002. For comparison, the Afar rift experienced 14 dyke intrusion events between 2005 and 2009 (Belachew *et al.* 2011) with individual earthquake swarms lasting between 0.5 and 5 days. At Krafla volcano in Iceland, 20 seismic sequences, connected with the inflation and deflation of a magma chamber, were observed between 1975 and 1984 (see Buck *et al.* 2006 for a review of this and similar cyclic dyking episodes in Iceland and elsewhere).

5 DISCUSSION

5.1 Swarms as indicators for dyking events

While the above criteria correlate seismic swarm activity in time and space to magmatic structures they cannot yield direct evidence for ongoing magmatic intrusion. The observation of intrusion tremor and migration of earthquake hypocentres, in contrast, are considered clear indicators of dyke propagation (Bohnenstiehl & Dziak 2008) and have been used to infer spreading events at mid-ocean ridges, for example, at Axial Volcano on the Juan de Fuca Ridge (Fox *et al.* 1995). On land, the Krafla dyking episode has impressively demonstrated the relation between migrating seismicity and the

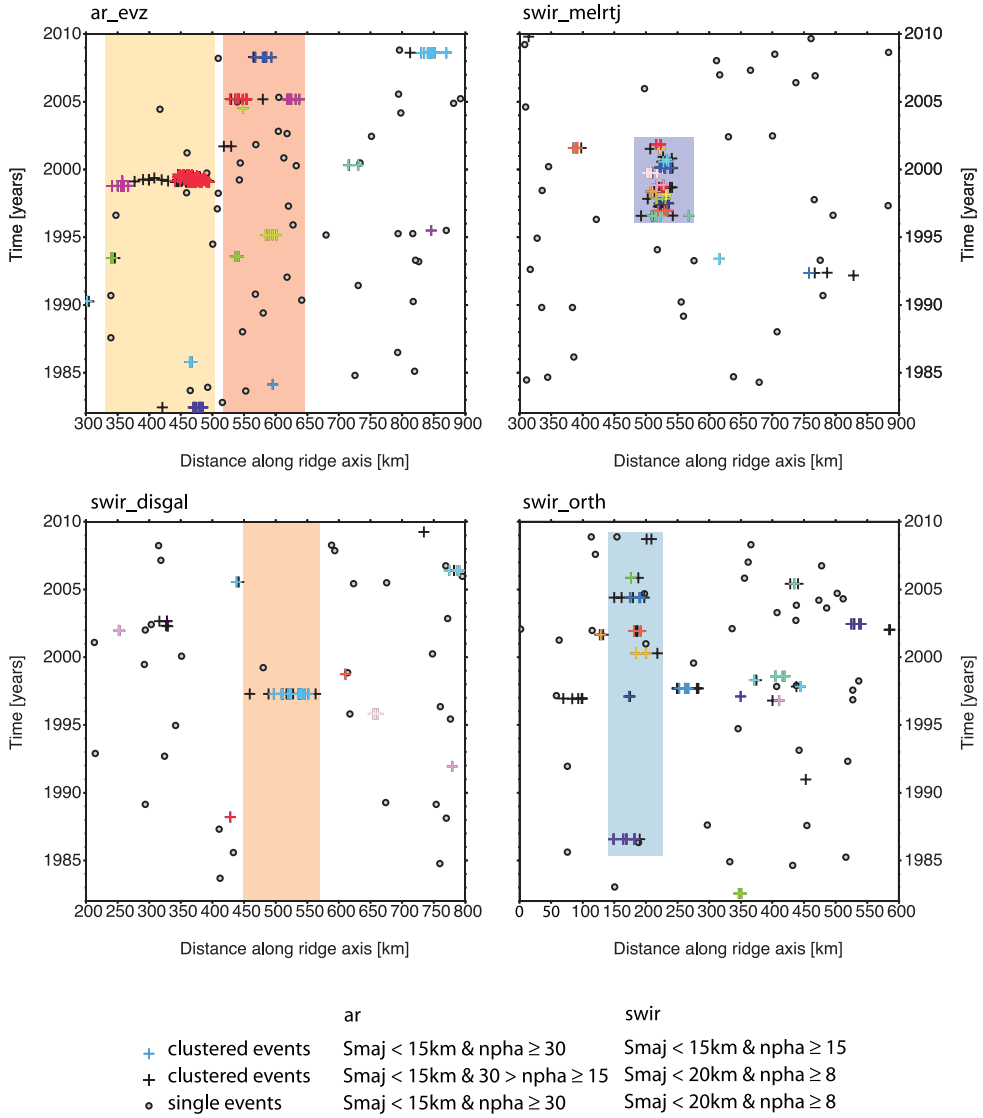

Figure 8. Close-up of Fig. 3 for sections with spatially extended (left-hand side) and temporally repeated (right-hand side) swarm activity. The plot scale of all sections is identical. Crosses mark all kinds of clustered events (swarms and sequences) and circles mark single events. Only events that fulfil the indicated location quality criteria are included. Coloured crosses refer to well-located event clusters, arbitrary colours are used to distinguish the clusters. Reddish boxes in the left plots mark the along-axis extent of rift axis activated in one or several nearly contemporaneous clusters (top panel). Bluish boxes indicate the space and time limits of repeated swarm activity. Note the 7 yr of periodic swarm activity in a narrow region of swir_melrtj.

propagating dyke tip (Brandsdóttir & Einarsson 1979). Another example is the recent Eyjafjallajökull eruption where microearthquakes traced the ascending magma (Tarasewicz *et al.* 2012). However, the seismicity produced by cracking at the tip of a propagating dyke is of low magnitude (Rubin & Gillard 1998) unable to be detected at teleseismic distances. Instead, the stress imposed by the dyke emplacement may cause pre-existing faults on top and ahead of the dyke to fail producing larger earthquakes (Rubin 1992). In this case, however, an earthquake migration pattern may be less clear if fault failure is not triggered instantaneously by the dyke.

At teleseismic distances, it is therefore not reasonable to require a clear migration of epicentres in a swarm as an indicator for a magmatic origin of a swarm. A prominent example of a seismic swarm observed at teleseismic distances occurred at the Lucky Strike segment of the MAR. Dziak *et al.* (2004) detected an earthquake sequence in hydroacoustic data which qualified as a dyke emplacement swarm as it was accompanied by volcanic tremor. This swarm lasted for 29 hr and contained 33 earthquakes of $3.3 < m_b < 5.0$ detected by land seismometers, the only teleseismic swarm of its kind in 20+ yr. The swarm had two larger earthquakes at its beginning, the remaining teleseismic earthquakes occurred 5.5 hr later when most of the 147 hydroacoustically detected smaller events had already taken place. The seismicity did not propagate, but a ridge section of about 80 km length was activated instantaneously. Dziak *et al.* (2004) interpret the Lucky Strike swarm as reflecting dyke intrusion into the shallow crust with low magnitude hydroacoustic events at the beginning of the swarm, followed by segment-scale normal faulting in large teleseismic events to adjust to the stress perturbation caused by magmatic intrusion. A spatial relation between the dyke location and epicentres of the teleseismic earthquakes could not be established.

In their teleseismic study of earthquakes swarms at the MAR, Bergman & Solomon (1990) require a swarm to show a significant

along-axis extent typical for lateral dyke intrusion events to qualify for a magmatic versus a purely tectonic origin. They identified more than 30 swarms, defining a swarm as a cluster of three or more earthquakes. Applying the 8+ events definition of a swarm as used here, the Bergman & Solomon (1990) data set then only counts five swarms, all of which lasted for several days, showed considerable along-axis seismic activation and belonged therefore to the group of swarms which shared characteristics with seismic swarms accompanying dyking episodes observed on land.

In their recent study of hydroacoustically observed seismic swarms at the northern MAR, Goslin *et al.* (2012) note that swarm-type seismic sequences without a mainshock are predominantly located on-axis at segment centres with mantle Bouguer anomaly lows and obvious volcanic structures. On this basis they infer a magmatic origin of the swarms.

None of the teleseismic swarms observed at ultraslow spreading ridges displays a classical epicentre migration pattern. However, considerable along-axis activation of faults was observed for several swarms, including the 1999 Gakkel swarm where a relation to a recent eruptive cycle could be established (Schlindwein & Riedel 2010). Comparing the seismicity of ultraslow spreading ridges to the analogues above, it appears reasonable to postulate a magmatic origin for the majority of the swarms.

5.2 Generation of large magnitude earthquakes in swarms at ultraslow spreading ridges

Dyke intrusion and volcanic eruptions typically go along with seismic swarms of magnitude 2–3. If associated with large deformation of a volcanic structure, magnitude 4–5 earthquakes may accompany eruptions or intrusions (McNutt 1996). For example, dyking episodes at the Afar rift were accompanied by a few earthquakes of magnitudes >4 (Afar, Belachew *et al.* 2011). Earthquakes of $M > 4$ in Iceland are confined to central volcanoes and their deflation whereas earthquakes associated with rifting and eruptions are smaller (Einarsson 1979). At ultraslow spreading ridges, however, earthquakes swarms appear to routinely include earthquakes with $M_u > 5.0$ (25 out of 27 swarms studied here, Table 3). The regional records of the Neumayer station showed that, in an observation period of 8 yr at swir_orth, all detected swarms featured teleseismically recorded events with $M_u \approx 5$ and no additional lower magnitude swarms were observed despite the reduced detection threshold ($m_b > 3.2$) compared to the teleseismic record (Läderach *et al.* this issue). In principle, the cold lithosphere at ultraslow spreading allows larger hypocentral depths and thus larger fault areas (Solomon *et al.* 1988), than at faster spreading ridges. It supports uncompensated high relief topography bounded by large faults (Cannat *et al.* 2003) prone to fail in high magnitude earthquakes. However, the relation of large earthquakes to the dyking process is more difficult to understand.

The model of Rubin (1992) suggests that dyke emplacement increases the least compressive stresses in the surrounding crust (apart from on top and ahead of the dyke) resulting in locking of the rift valley boundary faults. Tolstoy *et al.* (2001) applied this model to explain shallow earthquakes of the 1999 Gakkel earthquake swarm. Intensive relocation of these earthquakes, however, indicated that a large part of the events actually occurred at depths of about 15 km (Riedel & Schlindwein 2010) contradicting a locking of deep-reaching faults.

Toda *et al.* (2002) postulate that the seismicity rate and energy release of a swarm is related to the stressing rate produced by the dyke. Pedersen *et al.* (2007), however, analysed earthquakes and deformation during three well-studied dyking episodes in Iceland but could not confirm this relation. Rather, the seismic energy released during a dyke intrusion correlated with the background stress rate. On the basis of theoretical models, Rubin & Gillard (1998) attribute large earthquakes during swarms to faults that were loaded close to failure prior to dyke emplacement explaining the generation of large earthquakes in intrusions that followed a long period of quiescence. Here, however, $M_u > 5$ earthquakes are included in all repetitive swarms regardless of the preceding activity.

When modelling the changes in the stress field imposed by dyke intrusion, a symmetrical rift valley intruded centrally is usually assumed (Rubin 1992). At ultraslow spreading ridges, however, young volcanic structures are scattered across the rift valley including the flanks (Standish & Sims 2010). During the 1999 Gakkel volcanic episode there is evidence for hydrothermal and volcanic activity at both rift flanks (Schlindwein & Riedel 2010; Stranne *et al.* 2010). Standish & Sims (2010) therefore postulate that the large normal faults at ultraslow spreading ridges serve as pathways for magma transport. In addition, the volcanic centres at ultraslow spreading ridges are thought to pool melts from a larger region and feed these melts horizontally at crustal levels into the distal parts of the adjacent ridge segments (e.g. Sauter & Cannat 2010). Section ar_evz displays a remarkable zone of elevated seismic activity from about 75–100°E (km 350–650 in Fig. 5) with two examples of temporally related swarms at adjacent accretion sites (Fig. 8). This underlines that the swarm seismicity of ultraslow spreading ridges cannot be explained by a simple dyke intrusion model into a symmetric rift but that it rather results from a complex interplay of dyking and faulting at segment scale with fault-aided magma transport potentially playing an important role.

6 CONCLUSIONS

This study provides the first comprehensive analysis of the teleseismic earthquake swarms of ultraslow-spreading ridges. It uses 35 yr of globally recorded earthquakes along 7200 km of rift axis of the Arctic and SWIR systems and compares the seismicity patterns of 11 geologically different sections. As the cold, thick lithosphere of ultraslow spreading ridges is able to produce significant numbers of earthquakes detectable for seismometers on land, the teleseismic data set allowed helpful insights into active spreading processes at these ridges.

(1) Seismic swarms with eight or more events could be attributed to sites with clear indications of volcanic structures reaching from axial volcanic ridges, basaltic seafloor, pronounced magnetic and gravity signatures to off-axis volcanic ridges. The majority (24) of the 27 detected swarms could not be interpreted as tectonic mainshock–aftershock sequences. The swarms lasted between 1 day and 10 days with a few longer swarms. The swarms activated segments of >50 km length. Some swarms occurred repeatedly at specific sites over several years. The swarms at ultraslow spreading ridges released large amounts of seismic moment as they routinely triggered magnitude $M_u > 5$ events. This is confirmed by regional observations of swarms at the Orthogonal Supersegment by the Neumayer array in Antarctica. Despite its lower detection threshold it identified no intermediate magnitude swarms in addition to the teleseismically detected sequences.

(2) I infer that the majority of the swarms were triggered by magmatism and reflect a complex interplay between dyke

emplacement and activation of large normal faults able to produce $M > 5$ earthquakes.

(3) The 1999 earthquake swarm at the 85°E volcanic complex at eastern Gakkel ridge was the only earthquake swarm with unambiguous signs for contemporaneous magmatism. However, its duration, number of events and moment release were an order of magnitude larger than any of the other swarms. The swarm was interpreted to mark the onset of a volcanic cycle of at least 2 yr duration including deep submarine explosive activity, which has not yet been observed at other portions of ultraslow spreading ridges.

Due to the limitations of the teleseismic data set this study mainly provides an inventory of seismic swarm activity at ultraslow spreading ridges, describing observations and comparing them to spreading episodes at faster spreading ridges. Regional AuH monitoring complemented by dedicated local surveys of seismicity and lithospheric structure are sorely missing to fully understand the complex nature of magmatic spreading episodes at ultraslow spreading ridges and shed light on the role of large faults as magma pathways and the distribution mechanisms of magma along axis.

ACKNOWLEDGMENTS

I intensively used the online bulletin of the International Seismological Centre. I am indebted to C. Läderach and E. Korger for many fruitful discussions. Helpful comments to this manuscript were provided by I. Grevemeyer and two anonymous reviewers. This project was funded through the Emmy-Noether Program of the DFG under grant Schl 853/1–1.

REFERENCES

Belachew, M., Ebinger, C., Doté, D., Keir, D., Rowland, J.V., Hammond, J.O.S. & Ayele, A., 2011. Comparison of dike intrusions in an incipient seafloor-spreading segment in Afar, Ethiopia: seismicity perspectives, *J. geophys. Res.,* **116,** doi:10.1029/2010JB007908.

Bergman, E.A. & Solomon, S.C., 1990. Earthquake swarms of the Mid-Atlantic Ridge: products of magmatism or extensional tectonics?, *J. geophys. Res.,* **95,** 4943–4965.

Bohnenstiehl, D.R. & Dziak, R.P., 2008. Mid-ocean ridge seismicity, in *Encyclopedia of Ocean Sciences,* eds Steele, J., Thorpe, S. & Turekian, K., First Online Update, Academic Press, London.

Bown, J. & White, R., 1994. Variation with spreading rate of oceanic crustal thickness and geochemistry, *Earth planet. Sci. Lett.,* **121,** doi:10.1016/0012-821X(94)90082-5.

Brandsdóttir, B. & Einarsson, P., 1979. Seismic activity associated with the September 1977 deflation of Krafla Volcano in north eastern Iceland, *J. Volc. Geotherm. Res.,* **6,** 197–212.

Buck, W.R., Einarsson, P. & Brandsdóttir, B., 2006. Tectonic stress and magma chamber size as controls on dike propagation: constraints from the 1975–1984 Krafla rifting episode, *J. geophys. Res.,* **111,** B12404, doi:10.1029/2005JB003879.

Cannat, M., Rommevaux-Jestin, C., Sauter, D., Deplus, C. & Mendel, V., 1999. Formation of the axial relief at the very slow spreading Southwest Indian Ridge (49° to 69°E), *J. geophys. Res.,* **104,** 22825–22843.

Cannat, M., Rommevaux-Jestin, C. & Fujimoto, H., 2003. Melt supply variations to a magma-poor ultra-slow spreading ridge (Southwest Indian Ridge 61° to 69°E), *Geochem. Geophys. Geosys.,* **4**(8), 9104, doi:10.1029/2002GC000480.

Cannat, M., Sauter, D., Bezos, A., Meyzen, C., Humler, E. & Le Rigoleur, M., 2008. Spreading rate, spreading obliquity, and melt supply at the ultraslow spreading Southwest Indian Ridge, *Geochem. Geophys. Geosys.,* **9**(4), Q04002, doi:10.1029/2007GC001676.

Curewitz, D., Okino, K., Asada, M., Baranov, B., Gusev, E. & Tamaki, K., 2010. Structural analysis of fault populations along the oblique, ultra-slow spreading Knipovich Ridge, North Atlantic Ocean, 74°30'N-77°50'N, *J. Struct. Geol.,* **32,** 727–740.

Davis, S.D. & Frohlich, C., 1991. Single-link cluster analysis, synthetic earthquake catalogues, and aftershock identification, *Geophys. J. Int.,* **104,** 289–306.

DeMets, C., Gordon, R.G., Argus, D.F. & Stein, S., 1994. Effect of recent revisions to the geomagnetic reversal time scale on estimates of current plate motions, *Geophys. Res. Lett.,* **21,** 2191–2194.

Dick, H.J.B., Lin, J. & Schouten, H., 2003. An ultraslow-spreading class of ocean ridge, *Nature,* **426,** 405–412.

Dziak, R.P., Fox, C.G. & Schreiner, A.E., 1995. The June–July 1993 seismo-acoustic event at CoAxial segment, Juan de Fuca Ridge: evidence for a lateral dike injection, *Geophys. Res. Lett.,* **22,** 135–138.

Dziak, R.P., Smith, D.K., Bohnenstiehl, D.R., Fox, C.G., Desbruyeres, D., Matsumoto, H., Tolstoy, M. & Fornari, D.J., 2004. Evidence of a recent magma dike intrusion at the slow spreading Lucky Strike segment, Mid-Atlantic Ridge, *J. geophys. Res.,* **109,** B12102, doi:10.1029/2004JB003141.

Edmonds, H.N. *et al*., 2003. Discovery of abundant hydrothermal venting on the ultraslow-spreading Gakkel ridge in the Arctic Ocean, *Nature,* **421,** 252–256, doi:10.1038/nature01351.

Edwards, M., Kurras, G., Tolstoy, M., Bohnenstiel, D., Coakley, B. & Cochran, J., 2001. Evidence of recent volcanic activity on the ultraslow spreading Gakkel Ridge, *Nature,* **409,** 808–812, doi:10.1038/35057258.

Einarsson, P., 1979. Seismicity and earthquake focal mechanisms along the Mid-Atlantic plate boundary between Iceland and the Azores, *Tectonophysics,* **55,** 127–153.

Ekström, G., Dziewonski, A.M., Maternovskaya, N.N. & Nettles, M., 2005. Global seismicity of 2003: centroid-moment-tensor solutions for 1087 earthquakes, *Phys. Earth planet. Inter.,* **148,** 327–351.

Fox, C.G. & Dziak, R.P., 1998. Hydroacoustic detection of volcanic activity on the Gorda Ridge, February –March 1996, *Deep-Sea Res.,* **45**(II), 2513–2530.

Fox, C.G., Radford, W.E., Dziak, R.P., Lau, T.-K.A., Matsumoto, H. & Schreiner, A.E., 1995. Acoustic detection of a seafloor spreading episode on the Juan de Fuca Ridge using military hydrophone arrays, *Geophys. Res. Lett.,* **22,** 131–134.

Francis, T.J.G., 1968. The detailed seismicity of mid-oceanic ridges, *Earth planet. Sci. Lett.,* **4,** 39–46.

Frohlich, C. & Davis, S.D., 1990. Single-link cluster analysis as a method to evaluate spatial and temporal properties of earthquake catalogues, *Geophys. J. Int.,* **100,** 19–32.

Goslin, J. *et al*., 2012. Spatiotemporal distribution of the seismicity along the Mid-Atlantic Ridge north of the Azores from hydroacoustic data: Insights into seismogenic processes in a ridge–hot spot context, *Geochem. Geophys. Geosyst.,* **13,** Q02010, doi:10.1029/2011GC003828.

Grindlay, N.R., Madsen, J.A., Rommevaux-Jestin, C. & Sclater, J., 1998. A different pattern of ridge segmentation and mantle Bouguer gravity anomalies along the ultra-slow spreading Southwest Indian Ridge (15°30'E to 25°E), *Earth planet. Sci. Lett.,* **161,** 243–253.

International Seismological Centre, 2001. On-line bulletin, available at: http://www.isc.ac.uk (last accessed 2011 March 10).

Jakobsson, M., Macnab, R., Mayer, L., Anderson, R., Edwards, M., Hatzky, J., Schenke, H.-W. & Johnson, P., 2008. An improved bathymetric portrayal of the Arctic Ocean: implications for ocean modeling and geological, geophysical and oceanographic analyses, *Geophys. Res. Lett.,* **35,** doi:10.1029/2008GL033520.

Jokat, W. & Schmidt-Aursch, M.C., 2007. Geophysical characteristics of the ultraslow spreading Gakkel Ridge, Arctic Ocean, *Geophys. J. Int.,* **168,** 983–998.

Kanamori, H., 1977. The Energy Release in Great Earthquakes, *J. geophys. Res.,* **82,** 2981–2987.

Korger, E.I.M. & Schlindwein, V., 2012. Performance of localisation algorithms for teleseismic mid-ocean ridge earthquakes: the 1999 Gakkel ridge earthquake swarm, *Geophys. J. Int.,* **188,** 613–625.

Läderach, C., Korger, E., Schlindwein, V., Müller, C. & Eckstaller, A., Characteristics of tectono-magmatic earthquake swarms at the Southwest Indian Ridge between 16°E and 25°E, *Geophys. J. Int.,* doi:10.1111/j.1365-246X.2012.05480.x, in press (this issue).

Maus, S. *et al*., 2009. EMAG2: A 2–arc min resolution Earth Magnetic Anomaly Grid compiled from satellite, airborne, and marine magnetic measurements, *Geochem. Geophys. Geosyst.,* **10**(8), Q08005, doi:10.1029/2009GC002471.

McNutt, S.R., 1996. Seismic monitoring and eruption forecasting of volcanoes: a review of the state-of-the-art and case histories, in *Monitoring and Mitigation of Volcanic Hazards*, chapter 3, pp. 99–146, eds Scarpa, R. & Tilling, R., Springer-Verlag, Berlin.

Mendel, V., Sauter, D., Rommevaux-Jestin, C., Patriat, P., Lefebvre, F. & Parson L.M., 2002. Magmato-tectonic cyclicity at the ultra-slow spreading Southwest Indian Ridge: evidence from variations of axial volcanic ridge morphology and abyssal hills pattern, *Geochem. Geophys. Geosyst.,* **4**(5), 9102, doi:10.1029/2002GC000417.

Meyzen, C.M., Ludden, J.N., Humler, E., Luais, B., Toplis, M.J., Mével, C. & Storey, M., 2005. New insights into the origin and distribution of the DUPAL isotope anomaly in the Indian Ocean mantle from MORB of the Southwest Indian Ridge, *Geochem. Geophys. Geosyst.,* **6,** Q11K11, doi:10.1029/2005GC000979.

Michael, P.J. *et al*., 2003. Magmatic and amagmatic seafloor generation at the ultraslow-spreading Gakkel Ridge, Arctic Ocean, *Nature,* **423,** 956–961.

Mogi, K., 1963. Some discussions on aftershocks, foreshocks and earthquake swarms – the fracture of a semi-infinite body caused by an inner stress origin an its relation to the earthquake phenomena (Third Paper), *Bull. Earthq. Res. Inst.,* **41,** 615–658.

Müller, C. & Jokat, W., 2000. Seismic evidence for volcanic activity discovered in Central Arctic, *EOS Trans. Am. geophys. Un.,* **81,** 265–269.

Okino, K., Curewitz, D., Asada, M., Tamaki, K., Vogt, P. & Crane, K., 2002. Preliminary analysis of the Knipovich Ridge segmentation: influence of focused magmatism and ridge obliquity on an ultraslow spreading system, *Earth planet. Sci. Lett.,* **202,** 275–288.

Pedersen, R., Sigmundsson, F. & Einarsson, P., 2007. Controlling factors on earthquake swarms associated with magmatic intrusions; constraints from Iceland, *J. Volc. Geotherm. Res.,* **162,** 73–80, doi:10.1016/j.jvolgeores.2006.12.010.

Riedel, C. & Schlindwein, V., 2010. Did the 1999 earthquake swarm on Gakkel Ridge open a volcanic conduit? A detailed teleseismic data analysis, *J. Seismol.,* **14,** 505–522.

Rommevaux-Jestin, C., Deplus, C. & Patriat, P., 1997. Mantle Bouguer anomaly along an ultra-slow spreading ridge: implications for accretionary processes and comparison with results from Central Mid-Atlantic Ridge, *Mar. Geophys. Res.,* **19,** 481–503.

Rubin, A.M., 1992. Dike-induced faulting and graben subsidence in volcanic rift zones, *J. geophys. Res.,* **97**(B2), 1839–1858.

Rubin, A.M & Gillard, D., 1998. Dike-induced earthquakes: theoretical considerations, *J. geophys. Res.,* **103**(B5), 10017–10030.

Rundquist, D.V. & Sobolev, P.O., 2002. Seismicity of mid-oceanic ridges and its geodynamic implications: a review, *Earth-Sci. Rev.,* **58,** 143–161.

Ryan, W.B.F. *et al*., 2009. Global multi-resolution topography synthesis, *Geochem. Geophys. Geosyst.,* **10,** Q03014, doi:10.1029/2008GC002332.

Sauter, D., Patriat, P., Rommevaux-Jestin, C., Cannat, M. & Briais, A., 2001. The southwest indian ridge between 49°15'E and 57°E: focused accretion and magma redistribution, *Earth planet. Sci. Lett.,* **192,** 303–317.

Sauter, D., Mendel, V., Rommevaux-Jestin, C., Parson, L.M., Fujimoto, H., Mevel, C., Cannat, M. & Tamaki K., 2004a. Focused magmatism versus amagmatic spreading along the ultra-slow spreading Southwest Indian Ridge: evidence from TOBI side scan sonar imagery, *Geochem. Geophys. Geosyst.,* **5,** Q10K09, doi:10.1029/2004GC000738.

Sauter, D., Carton, H., Mendel, V., Munschy, M., Rommevaux-Jestin, C., Schott, J. & Whitechurch, H., 2004b. Ridge segmentation and the magnetic structure of the Southwest Indian Ridge (at 50°30'E, 55°30'E and 66°20'E): implications for magmatic processes at ultraslow-spreading centers, *Geochem. Geophys. Geosyst.,* **5**(5), Q05K08, doi:10.1029/2003GC000581.

Sauter, D. & Cannat, M., 2010. The ultraslow spreading Southwest Indian Ridge, in *Diversity of Hydrothermal Systems on Slow Spreading Ocean Ridges,* pp. 153–173, Geophysics Monograph 188, eds Rona, P.A. & Devey, C.W., American Geophysical Union, Washington, DC.

Schlindwein, V., Müller, C. & Jokat, W., 2005. Seismoacoustic evidence for volcanic activity on the ultraslow-spreading Gakkel Ridge, Arctic Ocean, *Geophys. Res. Lett.,* **32,** L18306, doi:10.1029/2005GL023767.

Schlindwein, V. & Riedel, C., 2010. Location and source mechanism of sound signals at Gakkel ridge, Arctic ocean: submarine Strombolian activity in the 1999–2001 volcanic episode, *Geochem. Geophys. Geosyst.,* **11**(1), Q01002, doi:10.1029/2009GC002706.

Scordilis, E.M., 2006. Empirical global relations converting M_S and m_b to moment magnitude, *J. Seismol.,* **10,** 225–236.

Simao, N., Escartín, J., Goslin, J., Haxel, J., Cannat, M. & Dziak, R., 2010. Regional seismicity of the Mid-Atlantic Ridge: observations from autonomous hydrophone arrays, *Geophys. J. Int.,* **183,** 1559–1578.

Smith, W.H.F. & Sandwell, D.T., 1997. Global seafloor topography from Satellite Altimetry and Ship Depth Soundings, *Science,* **277,** 1956–1962.

Smith, D.K., Escartin, J., Cannat, M., Tolstoy, M., Fox C.G., Bohnenstiehl, D.R. & Bazin, S., 2003. Spatial and temporal distribution of seismicity along the northern Mid-Atlantic Ridge (15°–35°N), *J. geophys. Res.,* **108**(B3), 2167, doi:10.1029/2002JB001964.

Snow, J.E., Hellebrand, E., von der Handt, A., Nauret, F., Gao, Y. & Schenke H.-W., 2011. Oblique nonvolcanic seafloor spreading in Lena Trough, Arctic Ocean, *Geochem. Geophys. Geosyst.,* **12,** Q10009, doi:10.1029/2011GC003768.

Sohn, R.A. *et al*., 2008. Explosive volcanism on the ultraslow-spreading Gakkel ridge, Arctic Ocean, *Nature,* **453,** doi:10.1038/nature07075.

Solomon, S.C., Huang, P.Y. & Meinke, L., 1988. The seismic moment budget of slowly spreading ridges, *Nature,* **334,** 58–60.

Standish, J.J. & Sims, K.W.W, 2010. Young off-axis volcanism along the ultraslow-spreading Southwest Indian Ridge, *Nat. Geosci.,* **3**(286), doi:10.1038/NGEO824.

Stranne, C., Sohn, R.A., Liljebladh, B. & Nakamura, K., 2010. Analysis and modeling of hydrothermal plume data acquired from the 85°E segment of the Gakkel Ridge, *J. geophys. Res.,* **115,** doi:10.1029/2009JC005776.

Sykes, L.R., 1967. Mechanism of earthquakes and nature of faulting on the Mid-oceanic ridges, *J. geophys. Res.,* **72,** 2131–2153.

Sykes, L.R., 1969. Seismicity of the mid-oceanic ridge system, in *The Earth's Crust and Upper Mantle,* pp. 148–153, Geophys. Monogr. 13, ed. Hart, P.J., American Geophysical Union, Washington, DC.

Sykes, L.R., 1970. Earthquake swarms and sea-floor spreading, *J. geophys. Res.,* **75,** 6598–6611.

Tarasewicz, J., Brandsdóttir, B., White, R.S., Hensch, M. & Thorbjarnardóttir, B., 2012. Using microearthquakes to track repeated magma intrusions beneath the Eyjafjallajökull stratovolcano, Iceland, *J. geophys. Res.,* **117,** doi:10.1029/2011JB008751.

Toda, S., Stein, R.S. & Sagiya, T., 2002. Evidence from the AD 2000 Izu islands earthquake swarm that stressing rate governs seismicity, *Nature,* **419,** 58–61.

Tolstoy, M., Bohnenstiel, D., Edwards, M. & Kurras, G., 2001. Seismic character of volcanic activity at the ultraslow-spreading Gakkel Ridge, *Geology,* **29**(12), 1139–1142, doi:10.1130/0091-7613(2001)029.

Tolstoy, M., Waldhauser, F., Bohnenstiehl, D.R., Weekly, R.T. & Kim, W.-Y., 2008. Seismic identification of along-axis hydrothermal flow on the East Pacific Rise, *Nature,* **451,** doi:10.1038/nature06424.

Toomey, D.R., Solomon, S.C., Purdy, G.M. & Murray, M.H., 1985. Microearthquakes beneath the Median Valley of the Mid-Atlantic Ridge near 23°N: hypocentres and focal mechanisms, *J. geophys. Res.,* **90,** 5443–5458.

Utsu, T., Ogata, Y. & Matsu'ura, R.S., 1995. The centenary of the Omori formula for a decay law of aftershock activity, *J. Phys. Earth,* **43,** 1–33.

Wolfe, C.J., Purdy, G.M., Toomey, R. & Solomon, S.C., 1995. Microearthquakes characteristics and crustal velocity structure at 29°N on the Mid-Atlantic Ridge: the architecture of a slow spreading segment, *J. geophys. Res.,* **100,** 24449–24472.

SUPPORTING INFORMATION

Additional Supporting Information may be found in the online version of this article:

Figure S1. Close-up map of section ar_knip showing swarm site 1. Left panel: Bathymetry with seismicity and moment tensor solutions. Middle panel: Bathymetry with features of swarm sites indicated. Green ellipse marks symmetric chain of off-axis highs. Right panel: EMAG2 magnetic anomaly map (Maus *et al.* 2009).
Figure S2. Map of section ar_wvz showing swarm site 2. Top panel: Bathymetry with seismicity and moment tensor solutions. Lower left panel: Bathymetry with swarm site indicated. Lower right panel: EMAG2 magnetic anomaly map with continuous CMA marked by orange ellipse.
Figure S3. Same as Fig. S2 but for section swir_orth with swarm site 7.
Figure S4. Close-up map of section swir_disgal showing swarm sites 8 and 9. Top panel: Bathymetry with seismicity and moment tensor solutions. Middle panel: Bathymetry with features of swarm sites indicated. Green arrow marks AVR, number indicates segment number after Cannat *et al.* (1999). Bottom panel: EMAG2 magnetic anomaly map (Maus *et al.* 2009) with circular CMA indicated by orange arrow and continuous CMA marked by orange ellipse.
Figure S5. Same as Fig. S4 but for section swir_galmel with swarm site 10. Green ellipse marks symmetric chain of off-axis highs.
Figure S6. Same as Fig. S5 but for section swir_melrtj with swarm sites 11 and 12.
Figure S7. Temporal development of the 27 swarms. Moment release (grey curve) and cumulative event number (coloured ramp with individual events as black circles) have been normalized and plotted versus the normalized swarm duration. Colours refer to sections, date and location of swarms on the rift axis are indicated. Potential mainshock–aftershock sequences with high a mainshock exceeding all other events by >0.5 magnitude units are marked with '*T*'.

Please note: Wiley-Blackwell are not responsible for the content or functionality of any supporting materials supplied by the authors. Any queries (other than missing material) should be directed to the corresponding author for the article.